International Journal on Interactive Design and Manufacturing (IJIDeM) (2024) 18:5261–5270
https://doi.org/10.1007/s12008-024-01835-w

TECHNICAL ARTICLE

Influence of electrode current on mechanical and metallurgical characteristics of hot wire TIG welded SS304HCu austenitic stainless steel and P91 ferritic steel dissimilar joints

S. Sravan Sashank[1] · S. Rajakumar[2] · R. Karthikeyan[3]

Received: 4 December 2023 / Accepted: 22 March 2024 / Published online: 16 April 2024

Abstract
The current work focusses on the effect of electrode current on the strength and metallurgical properties of hot wire TIG welded joints of SS304HCu austenitic stainless steel and P91 ferritic steel. The joints were developed with an electrode current of 134, 170, and 205 amperes at a constant heating current of 100 amperes and a wire feed speed of 1700 mm/min. A study of microhardness along the joint boundary was also carried out. Tensile properties of the welded joint were also studied to understand the effect of process parameters. As a result of this study, it was found that joints made at an electrode current of 170 amperes, a wire feed speed of 1700 mm/min and a heating current of 100 amperes showed a maximum tensile strength of 664 MPa compared to other joints. The microstructure of the interface was analyzed using optical microscopy. An EDS analysis was also carried out to understand the composition in the area of the interface. The microstructure of the welded joint's surface is directly related to the tensile strength of the joint.

Keywords Electrode current · Hot wire TIG · SS304HCu · P91 · EDS

1 Introduction

Most current research areas for advanced supercritical (AUSC) boilers are focused on combining improved materials. AISI 304HCu is a stainless steel variant that is increasingly favored for use in superheaters and reheaters. Austenitic steels are an excellent due to their strong corrosion resistance and oxidation. Additionally, these steels have exceptional creep qualities at temperatures exceeding 650ºC [1]. Nuclear power plants and reactors require materials that can withstand extremely high temperatures. Austenitic and ferritic-martensitic steels is preferred because of their wide application range and working environments. Boiler tubes are one known application for these materials. In the boiler section it is necessary to connect the superheater pipes, which helps to reduce overall costs [2]. Where a dissimilar connection is required, the superheater tubes are designed to be connected to header pipes [3]. Under these operating conditions, materials must withstand high temperatures while maintaining mechanical strength and microstructure stability. These materials are often joined using regular GTAW procedures. Nickel-based fillers or austenitic fillers are often used to join various compounds [4]. Cracks and microstructure heterogeneity are most common at joints because to variations in thermo-mechanical characteristics and carbon migration [5]. The elemental segregation produced by variation causes the introduction of thermal tensions. The temperature expansion coefficient of ferritic-martensitic stainless steels is lower compared to that of the austenitic steels [6].

✉ S. Sravan Sashank
sravansas@gmail.com

✉ S. Rajakumar
srkcemajor@yahoo.com

R. Karthikeyan
rkyen22@yahoo.com

[1] Department of Manufacturing Engineering, Annamalai University, Annamalai Nagar, Tamil Nadu 608 002, India

[2] Centre for Materials Joining and Research (CEMAJOR), Department of Manufacturing Engineering, Annamalai University, Annamalai Nagar, Tamil Nadu 608 002, India

[3] Department of Mechanical Engineering, Gokaraju Rangaraju Institute of Engineering and Technology, Bachupally, Hyderabad, Telangana 500 090, India

By adopting a variety of modern and unique procedures for combining this combination of materials, the problems can be resolved. Although nickel-based filler materials can make joints stronger, they can cause certain problems when the joints come together [7]. The main cause of the lower strength and microstructure heterogeneity was carbon migration at the contact. In this investigation, 1 mm diameter wire of grade ERNiCr-3 is used in the hot wire TIG welding method to link tubes made of 304HCu ASS and P91 ferritic steel. This method was first put forth, in which the wire supply is heated up before being supplied to the GTAW setup [8]. Because the wire feed is warmed, it is possible to preserve more of the energy of the developing arc. This procedure improves the bead profile and helps to raise the deposition rates. Any mix of materials can be joined using the method, which can be mechanised. Due to its lower initial investment requirements, this technique can quickly replace techniques which usually possess higher energy densities like laser beam and plasma arc welding [9]. The deflection can be decreased with the aid of induction and pulsed heating. Studies have suggested that the method of generating heat using heating current played a significant role on the rise in deposition rate [10]. It was also shown that they influence the welding bead geometry as well, and the primary shape changes were primarily associated with temperature distribution variations [11]. In comparison to cold wire, hot wire produces a better bead profile and a higher production rate [12]. HWGTAW created the most carbon depleted and enriched zones, as well as a large number of type I and type II borders [13]. Electrode current plays an important role in improving the joint quality. Recent study also revealed that the most influencing parameters are current and welding speed [14]. . The previous works on joining of these combination of materials are mainly done by using conventional TIG welding processes [15]. This work mainly focusses on finding the effect of electrode current on mechanical and microstructure characteristics of the dissimilar welded joints of SS304HCu ASS and P91 Ferritic Steel.

2 Materials and methods

The current investigation utilized 304HCu and P91 steel tubes. The study utilized base material tubes made of 304HCu ASS and P91 Alloy Steel, which had an outside diameter of 45 mm and a wall thickness of 9 mm. The chemical makeup of both materials underwent analysis utilising an X-ray fluorescence spectrometer. The composition of 304HCu austenitic stainless steel, P91 ferritic steel, and the joining material can be found in Table 1.

Figure 1 displays OM images of 304HCu austenitic stainless steel and P91 ferritic steel. The 304HCu ASS

Table 1 Chemical composition of base and filler material

wt %	Cr	Mo	Ni	Mn	Cu	C	Si	N	V	Nb	Ti	Fe
304HCu ASS	17.73	0.345	8.578	0.788	3.08	0.08	0.218	0.095	0.062	0.045		Balance
P91 Ferritic Steel	9.05	1.07	0.15	0.37		0.11	0.26		0.25	0.09		Balance
ERNiCr-3 Filler	21.27	0.94	Balance	3.2		0.06	0.28			2.15	0.15	2.57

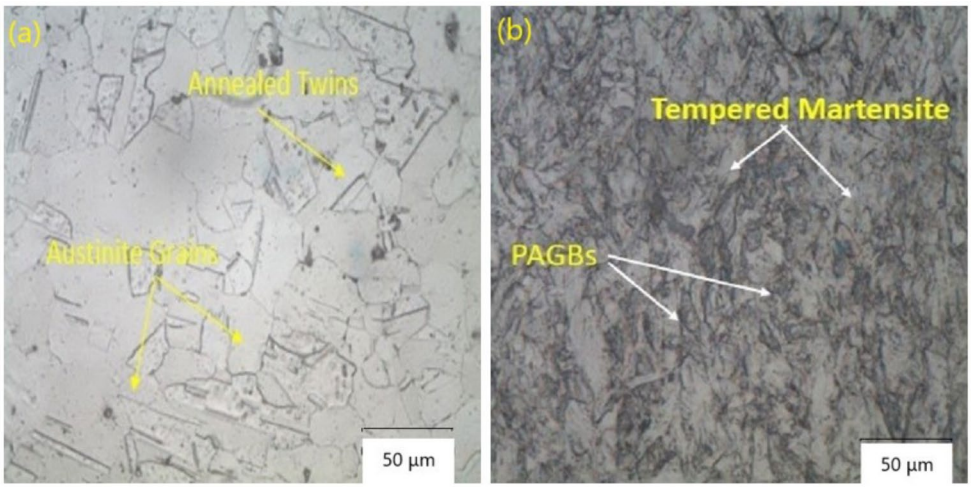

Fig. 1 Optical micrographs of (**a**) 304HCu ASS (**b**) P91 ferritic steel

Table 2 Mechanical properties of base materials

Material	UTS (MPa)	0.2% YS (MPa)	Elongation (%)	Hardness (VHN)
304HCu ASS	640	320	36	210
P91 Ferritic Steel	658	415	30	220

micrographs exhibited equiaxed polygonal austenite grains and annealed twins. The micrograph of P91 revealed the existence of a tempered martensitic microstructure along with preceding austenite grain boundaries (PAGB). Tensile specimens were prepared as per ASTM E8-19 and microhardness survey was carried out as per ASTM E92-17 standards. The mechanical characteristics of both materials are presented in Table 2.

Hot Wire TIG Welding is a technique that involves preheating the GTAW cold wire feed. This is done by passing a electric current over the wire, which heats it up through resistance, a process called Joule heating. An additional circuit is used for preheating, which harnesses the energy of the primary arc is greatly reduced. The wire was preheated to a temperature of 200ºC before it is fed to the wire pool [16]. The warmed wire allows for a faster deposition rate and produces a cleaner and more visually appealing bead profile. Preheating with pulsed current also helps to reduce deflection. This constraint was overcome by using induction heating. Tungsten Arc Hot Wire Welding was performed on P91 and 304HCu steel using a 1 mm diameter wire of grade ERNiCr-3, which is a filler substance composed primarily of nickel. The configuration of the welded joint is shown in the Fig. 2 below.

The experimental configuration has a specialized apparatus designed to securely grip and rotate pipes while performing welding operations. The tubes were precisely fabricated using a solitary V-groove at a precise angle of 60° along their edges. Prior to welding, the mating surfaces underwent thorough cleaning using acetone. The tube was supplied with argon shielding gas from both sides. The experimental configuration is depicted in Fig. 3. The welding process is primarily influenced by variables such as welding current, welding voltage, hot wire current, wire feed rate, welding speed, and wire positioning. To comprehend how process factors affect mechanical and metallurgical qualities, hot wire current (W), wire feed rate (F) and electro current (I) were chosen among these. The parameters of the hot wire

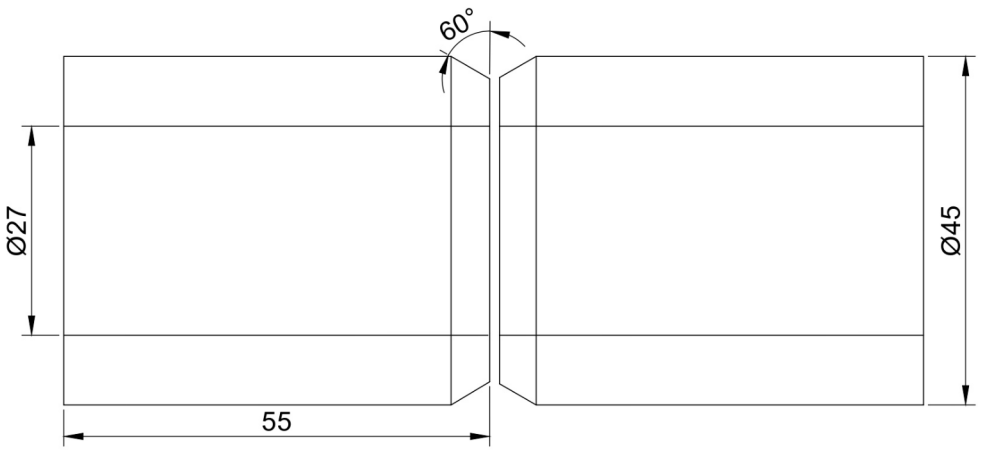

Fig. 2 Configuration of the welded joint

Fig. 3 Experimental Setup of HWGTAW

Table 3 Hot wire TIG welding process parameters

S. No	Electrode Current (amps)	Wire Feed Rate (mm/min)	Hot Wire Current (amps)
S1	134	1700	100
S2	170	1700	100
S3	205	1700	100

Fig. 4 Hot Wire TIG welded joints

TIG welding method that was utilised to join 304HCu ASS and P91 ferritic steel are shown in Table 3 below. The maximum (205 amps) and minimum (134 amps) value of the electrode current was established based on the inner side melt through and satisfactory bead appearance of the joints. The joints were prepared with the maximum, minimum and average values of the electrode current. The joints were fabricated for varying electrode currents of 134 amps, 170 amps and 205 amps, constant hot wire current of 100 amps and constant wire feed rate 1700 mm/min. A total of 4 passes were used to join the dissimilar materials. In Fig. 4, hot wire TIG welded joints are displayed.

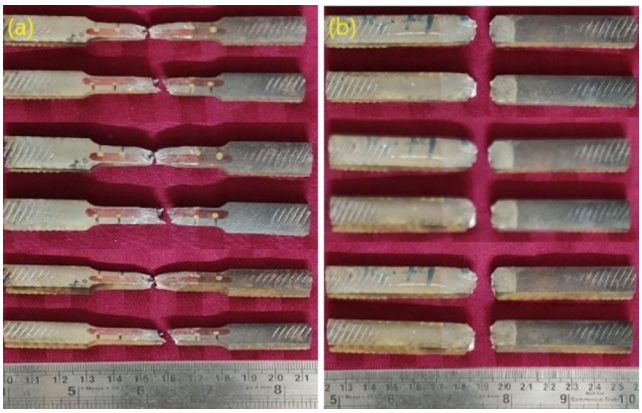

Fig. 5 Specimens after testing

Table 4 Mechanical Properties of Dissimilar Joints for Varying Electrode Current

Electrode Current (amps)	UTS (MPa)	0.2% YS (MPa)	Elongation (%)	Impact Toughness (J)
134	591	396	26	204
170	664	415	30	220
205	642	406	34	210

3 Results and discussions

3.1 Effect of electrode current on UTS & impact toughness

Tensile tests and impact tests for the dissimilar metal weld joints was performed at room temperature. ASTM E8-19 standard was used. The load-displacement curve was captured throughout the test and translated to an engineering stress-strain curve. The specimens after mechanical characterization are shown below in Fig. 5. The mechanical properties of dissimilar joints for varying process conditions are shown in the Table 4.

The data includes yield strength, ultimate tensile strength, percentage elongation, and toughness. The test samples were analyzed, and the average results together with their corresponding standard deviations are presented. The specimens exhibited failure in the vicinity of the base metal of P91. The fracture was situated around 3–4.5 mm away from the fusion contact of P91 and the weld metal. The tensile strength of the dissimilar metal weld joint is 1% greater than that of P91 ferritic steel and 3% greater than that of 304HCu ASS. Similar conclusions were drawn from the previous published works as well [13].

Electrode Current is one of the main process parameters for generating primary heat input in the hot wire TIG welding process [13]. . The range of parameters were fixed after conducting trail experiments and checking for deformities

in the joints. Joints were fabricated for various process conditions i.e. electrode current 134, 170 and 205 amps, wire feed rate 1700 mm/min and heating current 100 amps. As the electrode current rises there will be an increase in the heat energy. More material would be melted due to this. At lower electrode currents there will be a decrease in lack of penetration. The lower electrode current would not be adequate to cause the material to melt. An increase in electrode current leads to a corresponding increase in reinforcement, but it also results in a decrease in penetration. The relationship between electrode current and ultimate tensile strength is illustrated in Fig. 6. The Ultimate Tensile Strength (UTS) was estimated to be 664 MPa at 170 amps and 642 MPa at 205 amps. Lower electrode currents would lead to incomplete penetration and which couldn't hold the tensile load for longer duration of time. However, at higher currents there would be an excessive grain growth where the reinforcements would be machined off during the tensile test specimen preparation which would lead to a reduced cross-sectional area and a reduced load bearing capacity [17]. The joint strength would be higher at an electrode current of 170 amps and also a good geometry which helps in resisting higher loads for a long period of time. Macrostructures revealed that the joints fabricated with current of 134 amps and 205 amps had defects and the joints fabricated with 170 amps are defect free.

The specimens for impact tests were tested, and the average outcomes are shown. The impact toughness of P91 steel is reduced due to the existence of a carbon-enriched hard zone in the heat-affected zone (HAZ) as compared to other DMWJ sites. This phenomenon could be attributed to the migration of carbon transitioning from low chrome ferritic steel to high chromium steel. ERNiCr-3 side [18]. Carbon migration was not completely eliminated with Inconel fillers, but it will be substantially slowed as compared to chromium-rich stainless steel fillers [19]. The presence of Nb-rich carbide particles in Inconel filler, caused by the segregation of alloying elements along interdendritic boundaries, results in brittleness and reduced Charpy toughness of the weld metal due to the variability of process conditions. The enhancement in the mechanical properties were observed from the previous works as well [20] Table 4 displays the Charpy V-notch impact toughness at room temperature for dissimilar joints, under varied process conditions.

3.2 Effect of electrode current on microhardness

Figure 7 shows the microhardness variation across DMWJ at different levels of electrode current. The joints showed increased hardness at increased levels of electrode current. The hardness value increased with increase in process parameter values. The plastic deformation of the joint surface is reduced under tensile loading. Consequently, the joints' strength reduces as the parameter values increase. The selection of the optimal level of process parameters is important for obtaining excellent properties of dissimilar joints.

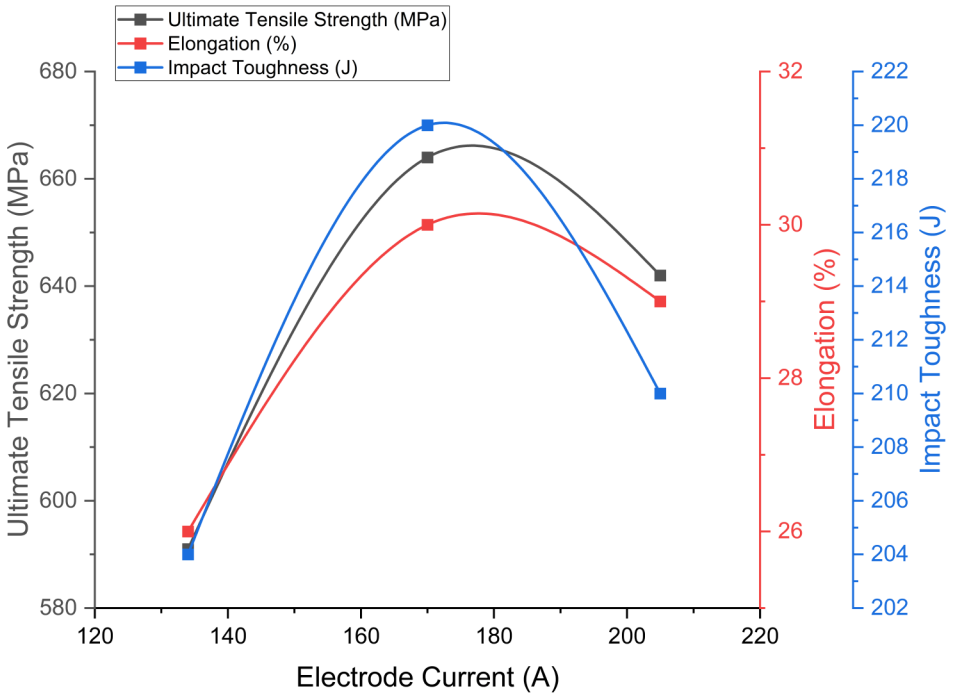

Fig. 6 Effect of electrode current on UTS & impact toughness

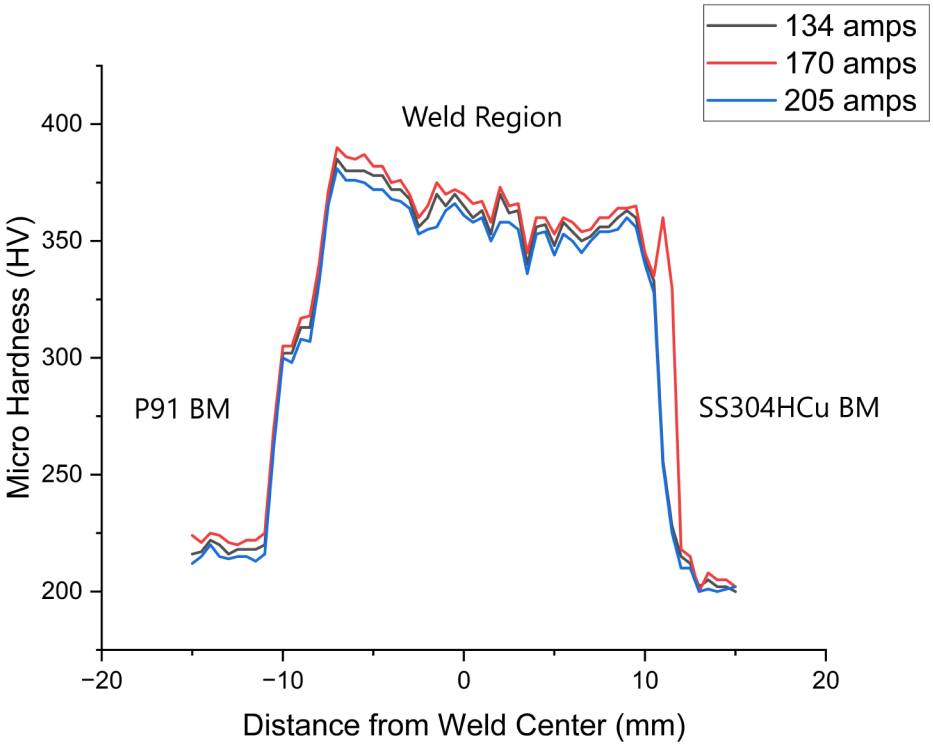

Fig. 7 Hardness Variation across the weld (**a**) S1@ 134 A (**b**) S2 @ 170 A (**c**) S3 @ 205 A

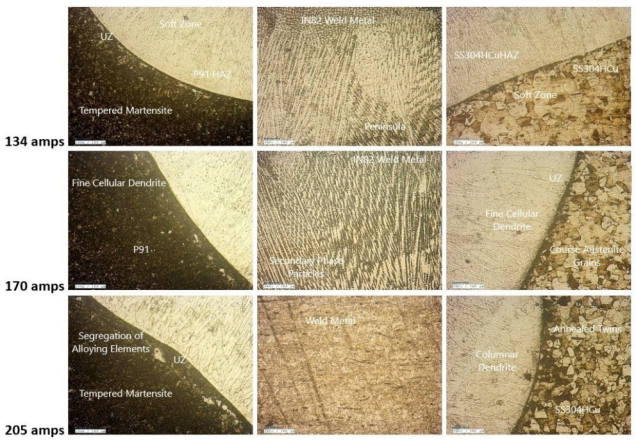

Fig. 8 Weld microstructure for the effect of electrode current

The hardness of the interface between P91 steel and filler metal reaches a maximum value of approximately 398 Hv. This can be attributed to the existence of a hard zone enriched with carbon, which is formed as a result of carbon migration. The outer edge of the heat-affected zone (HAZ), located 4–5 mm from the interface between P91 steel and filler metal, exhibits the lowest hardness of around 205 Hv. The HAZ of 304HCu ASS has higher hardness than the base material due to many multi-pass welding tempering cycles. An uneven distribution of hardness was seen in the DMWJ, as shown by the hardness survey. A zone of lower hardness, or weakest point, was identified near the outer edge of the heat-affected zone (HAZ).

3.3 Effect of electrode current on microstructure

Figure 8 shows the metallurgical features of TIG welded joints with hot wire. It shows the microstructure of welded joints at various electrode currents. The micrographs show the transformation of grains of austenitic base material into grains of delta-ferrite in an austenitic matrix. The weld metal solidifies in a strictly austenitic manner while P91 first solidifies as ferrite before changing into austenite and ultimately martensite.

An interface displaying tempered lath martensite was observed on the P91 side. Welding defects were observable at lower current values of 134 amps, and they adversely affected the mechanical qualities. For higher electrode current (specifically, 205 A), the microstructure in the fusion zone becomes more coarse. At greater levels of electrode current, the heat-affected area exhibits larger grain size. The fusion zone with a width of 170 A exhibits a heterogeneous shape. The presence of a delta ferrite structure enhances the ultimate tensile strength. The presence of austenitic structure, on the other hand, tends to raise the elongation percentage and there by yield strength increases. The formation of these is mainly attributed to the diffusion of carbon as reported in the previous research [21].

The SEM micrographs of the welded joints at different regions for varying electrode currents samples are depicted in Fig. 9. The hardened boundaries of the sub grains of the weld metal, which hardens in the form of an equiaxed

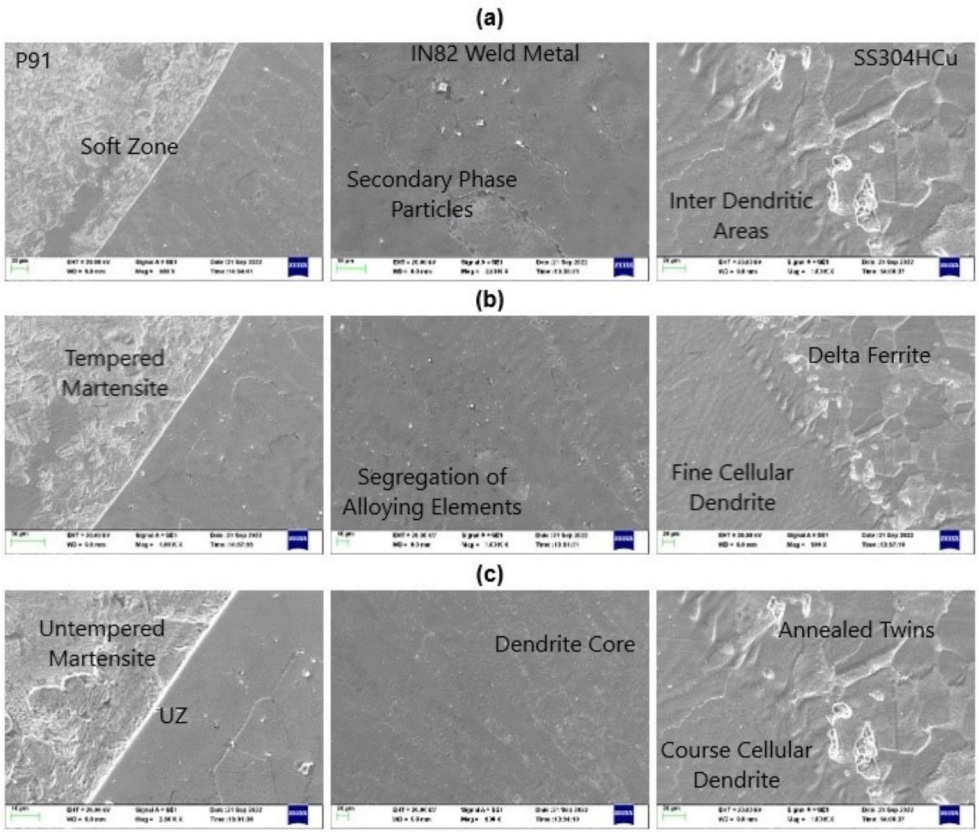

Fig. 9 SEM micrographs at various process conditions (**a**) S1@ 134 A (**b**) S2 @ 170 A (**c**) S3 @ 205 A

dendrite, give it a characteristic appearance The scanning electron microscope (SEM) image also illustrates the spatial distribution of the white particles along the boundaries. The sample S1 exhibits the presence of minuscule particles within the matrix, alongside the dendrite core area free of precipitates and the boundaries between dendrites. The presence of white particles at the interdendritic boundaries indicates significant segregation of C, Nb, and Mo. Secondary phase carbides are formed when the electrode current and heating current increase. Clear fusion boundaries and tempered martensite structure are visible at the contact between P91 and the filler metal. The crystallographic component of the solidified grain boundaries migrated away from the compositional component as a result of the decrease in electrode current and heating current. The unmixed zone, which has the same composition as 304HCu ASS base metal, is created when the 304HCu ASS base metal is completely melted and then resolidified.

3.4 EDS analysis

Figure 10 displays FE-SEM micrographs and the findings of an EDS study of the P91 HAZ (a). According to the EDS study, there is a higher Cr and Ni concentration content in the fusion zone near the weld fusion boundary than there is in P91.

Figure 10 (a) indicates that the weld fusion zone has an tempered martensitic structure (b). The chemical composition and microstructure at the fusion border of the 304Hcu ASS side weld were examined by FE-SEM and EDS analysis. The findings are presented in Fig. 10. Unlike the fusion boundary of the 304Hcu ASS weld, the heat-affected zone of the 304Hcu ASS was discovered to have high concentrations of chromium (Cr) and nickel (Ni).

3.5 Fracture surface analysis

The micrographs of the shattered surfaces were used to analyze the morphology of the fracture and kind of fracture in the weld joints, using a FE-SEM. The tensile test reveals broken surfaces in the joints, as well as the presence of dimples and microvoids. The specimens exhibited both ductile regions, characterized by dimples, and brittle regions, characterized by cleavage facets. Fracture surfaces may exhibit fine dimples and rip ridges. Figure 11 displays fractographs of S1, S2, and S3. The fracture surface pictures indicated that sample S1, which had a joint with low tensile strength, experienced a slightly brittle failure. Insufficient metallurgical bonding occurs due to inadequate electrode current and wire feed rates. Both samples S2 and S3 exhibit a ductile fracture mechanism, characterized by the presence of minuscule holes and depressions. A considerable amount

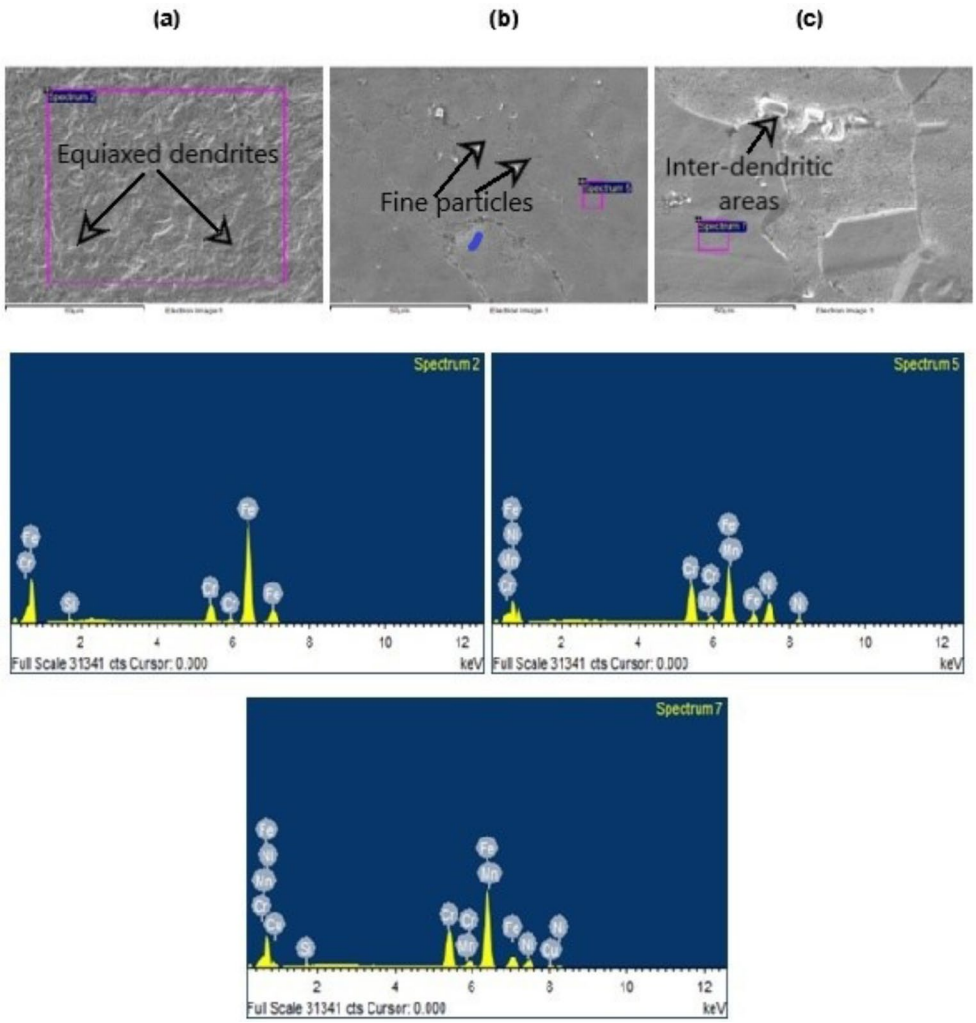

Fig. 10 FE-SEM micrographs and EDS Spectra of (**a**) P91 HAZ, (**b**) weld fusion zone and (**c**) 304HCu ASS HAZ

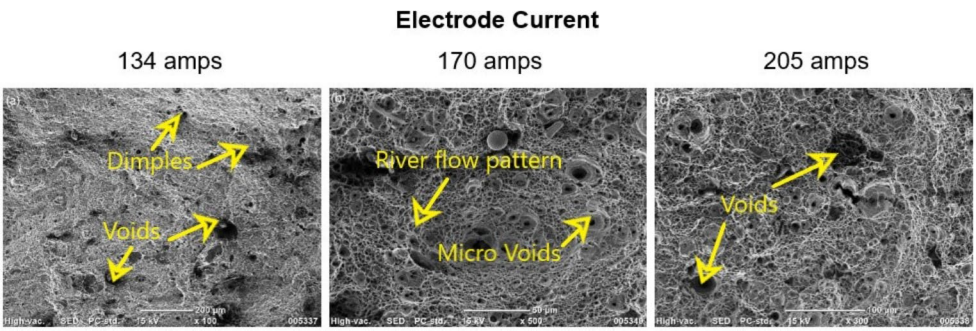

Fig. 11 SEM images of fractured tensile specimens (**a**) S1 (**b**) S2 (**c**) S3

of plastic distortion in sample S3 resulted in the production of a coarse grain structure, which can be attributed to the use of increased currents at the electrode, the heating current, and the wire feed rate.

4 Conclusions

An investigation was conducted to examine the influence of electrode current on the tensile strength, impact strength, hardness, and microstructure of dissimilar junctions between SS304HCu Austenitic Stainless Steel and P91 Ferritic Steel. The obtained results yielded the following conclusions.

1. Hot Wire TIG welding produced defect free dissimilar joints of 304HCu and P91 steel by varying the electrode current from 134 amps to 205 amps while wire feed rate 1700 mm/min and heating current 100 amps kept constant.
2. The electrode current significantly impacted the mechanical qualities of the joints, whereas the heating current and wire feed rate influenced the stability of the joint.
3. The Joints produced a peak ultimate tensile strength of 664 MPa when subjected to an electrode current of 170 amps, a wire feed rate of 1700 mm/min, and a heating current of 100 amps.
4. A difference in hardness was measured across the dissimilar joints. A peak hardness of 398 Hv is observed at the interface of P91 steel and filler metal, while the outside edge of 304HCu ASS HAZ has the lowest measured hardness value of 205 Hv.
5. By examining the elemental spectrum using EDS analysis, it was possible to clearly illustrate the disparity in atomic mass of the alloying elements. The study revealed that the SS304HCu-P91 joints' contact region contains diffusion components.
6. The tensile fracture surfaces of all the samples were primarily characterized by ductile dimples accompanied by tear ridges, indicating significant plastic deformation before complete failure.

Declarations

Competing interests The authors declare that they have no known competing financial interests or personal relationships that could have appeared to influence the work reported in this paper

References

1. Ravibharath, R., Muthupandi, V., Srinivasan, P.B., Devakumaran, K.: Characterization of solidification cracking in 304HCu austenitic stainless steel welds. Trans. Indian Inst. Met. **73**, 2345–2353 (2020). https://doi.org/10.1007/s12666-020-02028-1
2. Vekeman, J., Huysmans, S., de Bruycker, E.: Weldability assessment and high temperature properties of advanced creep resisting austenitic steel DMV304HCu. Weld. World. **58**, 873–882 (2014). https://doi.org/10.1007/s40194-014-0166-3
3. Vinoth Kumar, M., Balasubramanian, V.: Effect of current pulsing on super 304HCu Weld joints. World J. Eng. **16**, 814–822 (2019). https://doi.org/10.1108/WJE-07-2019-0207
4. Sireesha, M., Shankar, V., Albert, S.K., Sundaresan, S.: Microstructural features of dissimilar welds between 316LN austenitic stainless steel and alloy 800. Mater. Sci. Eng. A. **292**, 74–82 (2000). https://doi.org/10.1016/S0921-5093(00)00969-2
5. Pandey, C., Mahapatra, M.M., Kumar, P., Saini, N.: Autogenous tungsten inert gas and gas tungsten arc with filler welding of dissimilar P91 and P92 steels. J. Press. Vessel Technol. **140**, 021407 (2018). https://doi.org/10.1115/1.4039127
6. Ganesan, V., Laha, K., Bhaduri, A.K.: Creep rupture properties of indigenously developed 304HCu austenitic stainless steel. Trans. Indian Inst. Met. **69**, 247–251 (2016). https://doi.org/10.1007/s12666-015-0779-2
7. Gong, Y., Cao, J., Ji, L.N., Yang, C., Yao, C., Yang, Z.G., Wang, J., Luo, X.M., Gu, F.M., Qi, A.F., Ye, S.Y., Hu, Z.F.: Assessment of creep rupture properties for dissimilar steels welded joints between T92 and HR3C, fatigue Fract. Eng. Mater. Struct. **34**, 83–96 (2011). https://doi.org/10.1111/j.1460-2695.2010.01496.x
8. Cheng, M., He, P., Lei, L., Xin Tan, X., Wang, Y., Sun, J., Li, Jiang, Y.: Comparative studies on microstructure evolution and corrosion resistance of 304 and a newly developed high mn and N austenitic stainless steel welded joints. Corros. Sci. **183**, 109338 (2021). https://doi.org/10.1016/j.corsci.2021.109338
9. Olivares, E.A., González, and Victor Manuel Vergara Díaz:. Study of the hot-wire TIG process with AISI-316L filler material, analysing the effect of magnetic arc blow on the dilution of the weld bead. *Welding international* 32, no. 2, 139–148 (2018). https://doi.org/10.1080/09507116.2017.1347327
10. Padmanaban, M.R., Anantha, B., Neelakandan, Kandasamy, D.: A study on process characteristics and performance of hot wire gas tungsten arc welding process for high temperature materials. Mater. Res. **20**(1), 76–87 (2017). https://doi.org/10.1590/1980-5373-MR-2016-0321
11. Kannan, P., Rajesh, V., Muthupandi, Devakumaran, K.: On the effect of temperature coefficient of surface tension on shape and geometry of weld beads in hot wire gas tungsten arc welding process. *Materials Today: Proceedings* 5, no. 2, 7845–7852 (2018). https://doi.org/10.1016/j.matpr.2017.11.465
12. Pai, A., Sogalad, I., Basavarajappa, S., Kumar, P.: Results of tensile, hardness and bend tests of modified 9Cr 1Mo steel welds: Comparison between cold wire and hot wire gas tungsten arc welding (GTAW) processes. Int. J. Press. Vessels Pip. **169**, 125–141 (2019). https://doi.org/10.1016/j.ijpvp.2018.12.002
13. Sirohi, S., Pandey, C., Goyal, A.: Role of the Ni-based filler (IN625) and heat-treatment on the mechanical performance of the GTA welded dissimilar joint of P91 and SS304H steel. J. Manuf. Process. **65**, 174–189 (2021). https://doi.org/10.1016/j.jmapro.2021.03.029
14. Cheng, M., et al.: Comparative studies on microstructure evolution and corrosion resistance of 304 and a newly developed high mn and N austenitic stainless steel welded joints. Corros. Sci. **183**, 109338 (2021). https://doi.org/10.1016/j.corsci.2021.109338
15. Harish, T.M., et al.: Assessment of microstructure and mechanical properties of keyhole plasma arc welded similar butt joint of AISI 304 H austenitic stainless steel. Mater. Res. Express. **6**(11) (2019). https://doi.org/10.1088/2053-1591/ab4e04
16. Ungethüm, T., et al.: Analysis of metal transfer and weld geometry in hot-wire GTAW with indirect resistive heating. Weld. World. **64**, 2109–2117 (2020). https://doi.org/10.1007/s40194-020-00986-0
17. Karthick, K., Malarvizhi, S., Balasubramanian, V., Krishnan, S.A., Sasikala, G.: Albert. Tensile and impact toughness properties of various regions of dissimilar joints of nuclear grade steels. Nuclear Eng. Technol. **50**(1), 116–125 (2018). https://doi.org/10.1016/j.net.2017.10.003
18. Sharma, P., Dheerendra Kumar Dwivedi: A-TIG welding of dissimilar P92 steel and 304H austenitic stainless steel: Mechanisms, microstructure and mechanical properties. J. Manuf. Process. **44**, 166–178 (2019). https://doi.org/10.1016/j.jmapro.2019.06.003
19. Muthusamy, C., Karuppiah, L., Paulraj, S., Kandasami, D., Kandhasamy, R.: Effect of heat input on mechanical and metallurgical properties of gas tungsten arc welded lean super martensitic stainless steel. Mater. Res. **19**, 572–579 (2016). https://doi.org/10.1590/1980-5373-MR-2015-0538

20. Kumar, R., et al.: Enhancement of mechanical properties through modified post-weld heat treatment processes of T91 and Super304H dissimilar welded joint. J. Manuf. Process. **78**, 59–70 (2022). https://doi.org/10.1016/j.jmapro.2022.04.008
21. Singh, G., et al.: Analysis and optimization of various process parameters and effect on the hardness of SS-304 stainless steel welded joints. *International Journal on Interactive Design and Manufacturing (IJIDeM), 1–8* (2023). https://doi.org/10.1007/s12008-023-01361-1